



Power Electronic Systems
Laboratory

© 2016 IEEE

Proceedings of the Conference „Advances in Magnetics“ (AIM 2016), Bormio, Italy, March 14-16, 2016

Thermal Analysis of a Bearingless Permanent Magnet Pump at Ultra-High Temperatures

T. Wellerdieck,
P. Peralta,
D. Steinert,
J. W. Kolar

This material is published in order to provide access to research results of the Power Electronic Systems Laboratory / D-ITET / ETH Zurich. Internal or personal use of this material is permitted. However, permission to reprint/republish this material for advertising or promotional purposes or for creating new collective works for resale or redistribution must be obtained from the copyright holder. By choosing to view this document, you agree to all provisions of the copyright laws protecting it.



Eidgenössische Technische Hochschule Zürich
Swiss Federal Institute of Technology Zurich

Thermal Analysis of a Bearingless Permanent Magnet Pump at Ultra-High Temperatures

Tobias Wellerdieck¹, Patricio Peralta¹, Daniel Steinert², and Johann W. Kolar¹

¹Power Electronic Systems Laboratory, ETH Zurich, Switzerland

²Levitronix GmbH, Zurich, Switzerland

wellerdieck@lem.ee.ethz.ch

Abstract—Bearingless pumps are used in a variety of applications with demand on low wear, high reliability and high purity.

High operation temperatures demand for special design considerations to ensure safe operation and long lifetime and require precise knowledge about the internal machine temperatures. In this paper, a lumped parameter model is used to determine the conductive heat transfer. The heat exchange with the environment is investigated with FEM calculations and approximate formulas. Temperature dependent analysis of the loss mechanisms and operation performance of the machine are also included. The calculations are verified with measurements on a prototype.

Index Terms—Bearingless machine, high temperature, thermal model, lumped parameter model.

I. INTRODUCTION

A bearingless machine is an electric motor with an integrated magnetic bearing. The integration of the bearing leads to a compact machine design. The rotor of a bearingless machine is suspended in a magnetic field, allowing for contact free levitation of the rotor [1].

The machine analyzed in this paper is a bearingless disc drive. This topology features passive stability in three degrees of freedom simplifying the bearing control [2]. The machine is used to drive a pump with a hermetically sealed pump head. The sealing and the absence of any mechanical bearing allows for very high purity, low contamination and long lifetime [3]. A photograph of a prototype is shown in Fig 1(a). The schematic view of the machine in Fig. 1(b) shows the sealed pump head and the compact design of the machine.

The analyzed pump will be operated with fluid temperatures exceeding 200 °C. The goal is to combine the aforementioned advantages of a bearingless machine with high thermal resilience. The high fluid temperatures and the internal machine losses will lead to high temperatures inside the machine and, subsequently, to high thermal stress on the machine components and materials. The selection of suitable components and materials requires precise knowledge of the internal machine temperatures at all operation conditions. A comprehensive analysis of the thermal effects in the machine is presented in this paper.

The drive and the bearing performance of a bearingless machine change with the temperature of the machine. This is mostly due to the demagnetization of the magnet at elevated temperatures. A physical explanation of this effect is included in section II.

The analysis of the machine temperatures is based on the study of the internal machine losses since these are, together with the hot fluid, the main heat sources in the machine. The

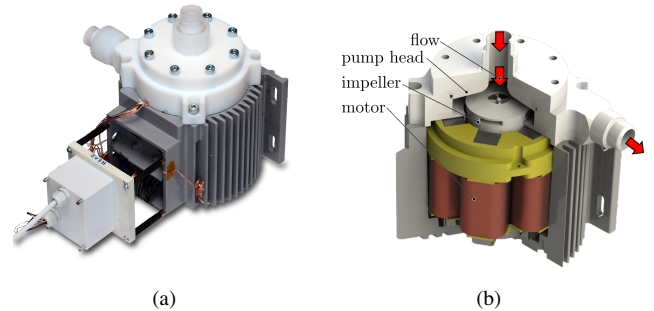


Fig. 1: Photography (a) and schematic view (b) of the bearingless ultra-high temperature pump.

focus lies on the modelling of the internal machine losses. The losses are dependent of the operation state of the machine and the internal machine temperatures. Therefore, a temperature dependent loss analysis is presented in section III.

The heat transfer inside the machine is approximated by a lumped parameter thermal model (LPTM). Such a model allows for a computational efficient calculation of the internal machine temperatures [4] and is well suited to analyze the impact of design variations. The LPTM is presented in section IV.

The loss analysis and the LPTM are verified using a machine prototype operated at different fluid temperatures. The results are shown in section V.

II. MACHINE PERFORMANCE

The bearing forces and the torque acting on the rotor are dependent on the machines temperature and can be calculated based on the magnetic flux density in the air gap [5], [6]. A schematic view of the motor is shown in Fig. 2(a). The torque acting on the rotor can be calculated as

$$T \approx c_D(\vartheta_m) \cdot I_D \propto \int_0^{2\pi} B_{\text{rad}}(\vartheta_m) B_{\text{tan}}(\vartheta_m) d\alpha \quad (1)$$

with c_D , ϑ_m , I_D , B_{rad} and B_{tan} being the torque constant, the magnet temperature, the drive current, the radial and tangential flux density in the air gap, respectively. The temperature dependency of the torque can be explained by analyzing the temperature dependency of the flux in the air gap

$$\vec{B}_a = \begin{bmatrix} B_{\text{rad}} \\ B_{\text{tan}} \\ B_z \end{bmatrix} = \begin{bmatrix} B_{\text{rad}} \\ B_{\text{tan}} \\ 0 \end{bmatrix}. \quad (2)$$

Note that the flux in z -direction is neglected due to symmetry.

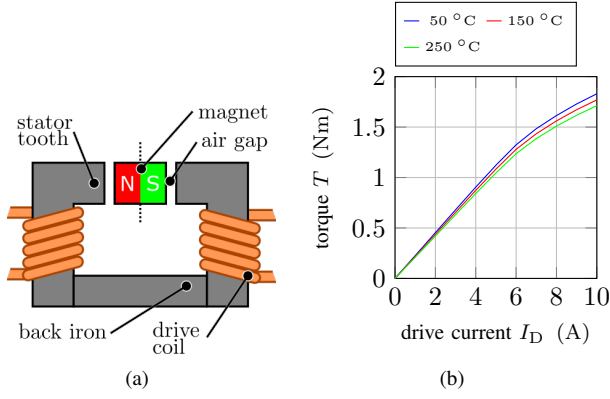


Fig. 2: Schematic view of a cut through the motor (the back iron is ring-shaped) (a) and simulated torque for different magnet temperatures (b).

This flux can be calculated as the superposition of the rotor field \vec{B}_r and the stator field \vec{B}_s as

$$\vec{B}_a(\vartheta_m) = \vec{B}_s + \vec{B}_r(\vartheta_m). \quad (3)$$

Rotor and stator field can be calculated independently of each other if the saturation of the iron is neglected.

The stator field is only dependent on the drive current I_D , the geometry of the machine and the magnetic permeability of the iron $\mu_{r,Fe}$. The magnetic permeability of the iron is assumed to be constant since the machine is operated well below the curie temperature of iron at 700 °C [7].

The rotor field amplitude can be written as

$$|\vec{B}_r|(\vartheta_m) \propto B_{rem}(\vartheta_m) \quad (4)$$

with B_{rem} being the remanence flux density of the magnet. Rare earth magnets, such as Neodymium-Iron (NdFe) or Samarium-Cobalt (SmCo), exhibit demagnetization at elevated temperatures. The most temperature resilient SmCo magnets have demagnetization coefficients in the range of 0.03 – 0.115 %/°C, depending on the temperature and the grading of the magnet [8].

The rotor field is weakened if the temperature of the magnet is increased, therefore, the torque constant has a negative temperature dependency

$$\frac{\partial c_D}{\partial \vartheta_m} < 0. \quad (5)$$

A FEM simulation was used to simulate the torque for different magnet temperatures. Figure 2(b) shows the torque over drive current in the range of 0 to 10 A_{RMS} for different magnet temperatures.

The bearing forces are also dependent on the air gap field and can be calculated similarly to the torque. Therefore, the bearing force constant c_B shows the same temperature dependency as the torque constant c_D .

A machine with hot magnet requires higher drive and bearing currents to generate the same bearing forces and torque as a cold machine due to the reduced force and torque constants.

III. LOSS ANALYSIS

The internal machine losses are, together with the heating from the fluid, the main heat sources in the machine. The losses of a permanent magnet machine can be split into copper losses P_{Cu} and iron losses P_{Fe} . The latter are further divided into hysteresis losses $P_{Fe,Hy}$ and eddy current losses $P_{Fe,Ed}$ [9].

The temperature in the coils is unevenly distributed. Therefore, the copper losses of the i -th turn $P_{Cu,i}$ is calculated as

$$P_{Cu,i} = I_D^2 \frac{l_i}{A_{Cu}} \rho_{Cu,RT} \left(1 + \alpha_{Cu} (\vartheta_{Cu,i} - \vartheta_{RT}) \right) \quad (6)$$

and the total copper losses as

$$P_{Cu} = \sum_{i=1}^N P_{Cu,i} \quad (7)$$

with N, l_i and A_{Cu} being the number of turns, the length of wire of the i -th turn and the copper area and $\rho_{Cu,RT}, \alpha_{Cu}, \vartheta_{Cu,i}, \vartheta_{RT}$ being the resistivity of copper at room temperature, the temperature coefficient of the electric resistivity of copper, the temperature of the i -th turn and the room temperature respectively.

The stator iron exhibits inhomogeneous flux density and temperature distribution. Therefore, it is split up into M parts with approximately homogeneous flux density amplitudes and temperature distribution in each part. The i -th part has the flux density amplitude \hat{B}_i , the temperature $\vartheta_{Fe,i}$ and the mass m_i . Figure 3(b) shows the first four segments in the stator tooth for a drive current of 5 A. The segmentation varies for different drive currents and temperatures due to the saturation of the iron.

The total iron losses are calculated with the Steinmetz equation as

$$\begin{aligned} P_{Fe,Ed} &= \sum_{i=1}^M c_{Ed}(\vartheta_{Fe,i}) \cdot f^{\alpha_{Ed}} \cdot \hat{B}_i(\vartheta_{Fe,i})^{\beta_{Ed}} \cdot d_{Fe}^2 \cdot m_{Fe,i} \\ P_{Fe,Hy} &= \sum_{i=1}^M c_{Hy} \cdot f^{\alpha_{Hy}} \cdot \hat{B}_i(\vartheta_{Fe,i})^{\beta_{Hy}} \cdot m_{Fe,i} \\ P_{Fe} &= P_{Fe,Ed} + P_{Fe,Hy} \end{aligned} \quad (8)$$

with d_{Fe} being the thickness of the iron sheets, f being the frequency of the oscillating field and $c_{Ed}, c_{Hy}, \alpha_{Ed}, \alpha_{Hy}, \beta_{Ed}, \beta_{Hy}$ being the parameters of the Steinmetz equation. Only the eddy current loss constant is temperature dependent. It is approximated as

$$c_{Ed}(\vartheta) = \frac{c_{Ed,RT}}{1 + \alpha_{Fe}(\vartheta - \vartheta_{RT})} \quad (9)$$

with $c_{Ed,RT}$ being the Steinmetz parameter for the eddy current losses at room temperature and α_{Fe} the temperature coefficient of the electric resistivity of the iron. The parameters were found by fitting (8) to loss measurements of the stator iron material obtained from the manufacturer.

The determination of the flux density amplitudes \hat{B}_i in different parts of the stator iron was conducted with the use

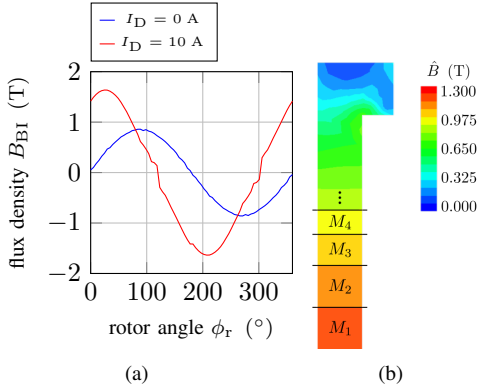


Fig. 3: Flux density at a fixed position in the back iron for one rotation of the rotor with variation of the drive current I_D at room temperature (a) and segmentation of the stator tooth for $I_D = 5$ A.

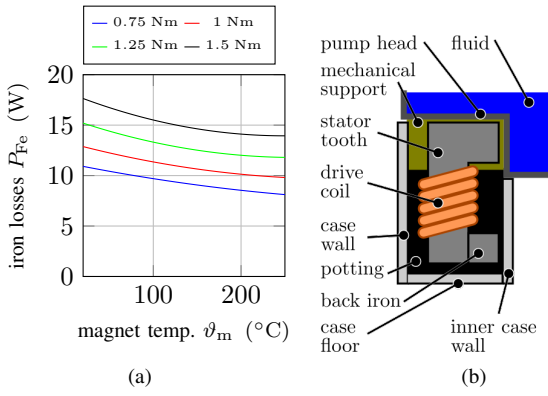


Fig. 4: Iron Losses at $n = 6000$ rpm with fixed torque for different magnet temperatures ϑ_m (a) and schematic view of the pump showing the temperature points utilized in the LPTM (b)

of a FEM simulation. Only the analysis of the back iron is shown in the following.

Figure 3(a) shows the flux density at a fixed point in the back iron for one full rotor rotation, the rotor angle is labeled ϕ_r . The amplitude of the flux density is dependent on the drive current I_D . The flux is sinusoidal, which is a requirement for the application of (8).

Figure 4(a) shows the iron losses P_{Fe} if the machine is operated at $n = 6000$ rpm with a drive torque of $T = 0.75 - 1.5$ Nm at different temperatures. The drive current is adjusted to counteract the demagnetization of the magnet. The analysis shows that the change in loss is up to 25 %. This is mainly due to the reduced conductivity of the stator iron.

IV. THERMAL MODEL

The temperature distribution inside the machine is calculated using an LPTM. A total of eight temperature points are defined inside the machine. Figure 4(b) shows a cut through the machine, the temperature points are labeled.

Internal losses are modeled with heat sources. Fixed temperatures, such as the fluid and the ambient temperature, are converted to equivalent heat sources.

Heat transfer inside the model is approximated with thermal admittances, taking the conductive heat transfer in solids as

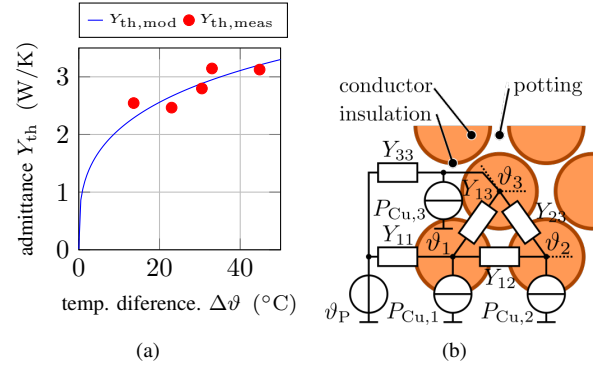


Fig. 5: Measured and calculated thermal convective heat exchange to the ambient (a) and schematic representation of the winding (b).

well as the convective and radiative heat exchange with the ambient air into account. Models for the conductive heat transfer in solids and radiative heat transfer to the ambient are available in the literature [10].

The modelling of the convective heat transfer from the machine case surface to the ambient is more challenging. In this paper, an approximate formula for the convective heat transfer from a horizontal cylinder is used. The approximate convection coefficient $\alpha_{c,approx}$ is calculated based on the radius of the case r_c , the case temperature ϑ_c and the ambient temperature ϑ_a as

$$\alpha_{c,approx} = \frac{\lambda}{\pi \cdot r_c} \left(0.752 + 0.387 (Gr \cdot Pr \cdot f(Pr))^{1/6} \right)^2$$

$$Gr = \frac{g(\pi \cdot r_c)^3}{\nu^2} \beta (\vartheta_c - \vartheta_a)$$

$$f(Pr) = \left(1 + \left(\frac{0.559}{Pr} \right)^{9/16} \right)^{-16/9}$$
(10)

with the material dependent thermal conductivity λ , the Prandtl number Pr , the kinematic viscosity ν and the thermal expansion coefficient β [11]. The approximate formula can be evaluated with little computational effort. A 2D-FEM simulation was used to analyze the effect of the case fins. A fin-correction factor ζ was calculated for a limited number of points. The thermal admittance, $Y_{th,mod}$ is

$$Y_{th,mod} = \zeta \cdot \alpha_{c,approx} \cdot A_{conv} \quad (11)$$

with A_{conv} being the case surface. The convective heat transfer was also measured by applying a DC current to the drive coils of the machine to heat the machine. The convective heat transfer can then be calculated by measuring the input power P_{in} , the case temperature and the ambient temperature. The measured thermal admittance is

$$Y_{th,meas} = \frac{P_{in}}{\vartheta_c - \vartheta_a} \quad (12)$$

The radiative heat transfer to the ambient air is neglected. Figure 5(a) shows the measured thermal admittance $Y_{th,meas}$ and the corrected thermal admittance $Y_{th,mod}$. The corrected approximate calculation matches the measured heat transfer.

The temperature in the windings is modelled in two ways.

TABLE I: Temperatures in the winding with 200 °C fluid temperature.

drive current	$\vartheta_{w,\min}$	$\vartheta_{w,\text{mean}}$	$\vartheta_{w,\max}$
0 A	64.5 °C	67.8 °C	76.1 °C
5 A	69.7 °C	75.6 °C	84.7 °C
10 A	85.9 °C	100.7 °C	112.7 °C

The simple model assumes that the winding temperature is constant over the whole winding. This simplifies the calculation of the thermal admittances and keeps the complexity of the model low. This model is used for the verification in section V. However, it is obvious that the winding temperature will not be homogeneous. Windings at the surface of the coil tend to be cooler than windings in the middle. The second modelling approach splits the winding into turns and the temperature at each turn is calculated. The heat transfer from turn to turn is calculated with thermal admittances [12]. The temperature of the i -th turn of the winding $\vartheta_{Cu,i}$ is used to evaluate the copper losses according to (7). Figure 5(b) shows a part of the winding model with the turn temperatures $\vartheta_1, \vartheta_2, \vartheta_3$, the potting temperature ϑ_P and the copper losses per turn $P_{Cu,1}, P_{Cu,2}, P_{Cu,3}$. The admittance Y_{ij} labels the thermal admittance from turn i to turn j .

Table I shows the surface winding temperature $\vartheta_{w,\min}$, the mean winding temperature $\vartheta_{w,\text{mean}}$ and the maximum winding temperature $\vartheta_{w,\max}$ for different drive current amplitudes in a machine with 200 °C fluid temperature. The difference in temperatures at zero drive current is due to the inhomogeneous heating by the fluid. Nonzero drive currents exacerbate this effect since hotter winding turns will have a higher ohmic resistance and generate more losses. Turns in the middle of the winding are more than 25 °C hotter than turns on the surface. This effect must be accounted for when selecting the conductor and insulation materials.

V. VERIFICATION

A prototype of the bearingless pump is used to verify the thermal model, cf. Fig. 1(a). PT1000 elements were added in order to measure the internal machine temperatures during operation. The prototype was run in a hydraulic test set-up using silicon oil with controlled oil temperature. Table II shows the predicted and the measured temperatures and the relative errors for fluid temperatures of 200 °C and 220 °C.

TABLE II: Verification of the thermal model for 200 °C and 220 °C fluid temperature.

position	model	measurement	error
oil		220 °C	
ambient		50 °C	
coil surface	81.3 °C	83 °C	2 %
stator back iron	83.8 °C	83 °C	1 %
stator iron tooth	91.1 °C	91 °C	0,1 %
mechanical support	161.8 °C	160 °C	1.1 %
case	76.4 °C	70 °C	8 %
oil		200 °C	
ambient		45 °C	
coil surface	67.2 °C	66 °C	1.9 %
stator back iron	68.2 °C	66 °C	3.2 %
stator iron tooth	72.2 °C	72 °C	0.3 %
mechanical support	154.4 °C	153 °C	0.9 %
case	64 °C	60 °C	6.21 %

The verification shows that the model allows the prediction of the internal machine temperatures with acceptable precision. Therefore, the temperature distribution of the whole pump can be analyzed. Furthermore, the model allows the estimation of temperatures at points in the machine where no sensors can be mounted, eg. in the middle of the stator windings.

The case temperature shows the highest deviation between measured and estimated temperatures. This might be due to the fact that the machine is operated in an enclosure due to safety considerations. The enclosure has an impact on the airflow around the machine and the radiative heat transfer from and to the case surface. This effect could be captured by tuning the fin-correction factor ζ in (11) based on the measured values.

VI. CONCLUSION AND OUTLOOK

This paper gives an overview of the formulation of a LPTM for a bearingless pump. The model allows a computational efficient calculation of the internal machine temperatures and can be used as a basis for component and material selection and to analyze the impact on geometry variations on the internal temperatures. The paper shows that the temperature dependency of the iron and losses cannot be neglected and that modelling the stator winding with just one temperature is not sufficient due to the wide temperature distribution.

The temperature measurements show that the model is sufficiently accurate at the temperature range of interest.

VII. ACKNOWLEDGEMENT

This work was supported by the *Swiss Commission for Technology and Innovation CTI-KTI*.

REFERENCES

- [1] X. Sun, L. Chen, and Z. Yang, "Overview of bearingless permanent-magnet synchronous motors," *Industrial Electronics, IEEE Transactions on*, vol. 60, no. 12, pp. 5528–5538, 2013.
- [2] P. Karutz, T. Nussbaumer, and J. Kolar, "Magnetically levitated slice motors - an overview," in *Energy Conversion Congress and Exposition, 2009. ECCE 2009. IEEE*, pp. 1494–1501, Sept 2009.
- [3] R. Schöb, "Centrifugal pumps without bearing or seals," *World Pumps*, vol. 430, no. 12, pp. 34–37, 2002.
- [4] J. Nerg, M. Rilla, and J. Pyrhonen, "Thermal analysis of radial-flux electrical machines with a high power density," *Industrial Electronics, IEEE Transactions on*, vol. 55, pp. 3543–3554, Oct 2008.
- [5] B. Laptre, N. Takorabet, F. Meibody-Tabar, J. Fontchastagner, R. Lateb, and J. D. Silva, "New model of radial force determination in bearingless motor," *IEEE Transactions on Magnetics*, vol. 51, pp. 1–4, March 2015.
- [6] T. Wellerdieck, T. Nussbaumer, and J. Kolar, "Angle-sensorless zero- and low-speed control of bearingless machines," *IEEE Transactions on Magnetics*, vol. PP, no. 99, pp. 1–1, 2016.
- [7] N. Takahashi, M. Morishita, D. Miyagi, and M. Nakano, "Examination of magnetic properties of magnetic materials at high temperature using a ring specimen," *IEEE Transactions on Magnetics*, vol. 46, pp. 548–551, Feb 2010.
- [8] VAC-Vacuumschmelze, "SELTEN-ERD-DAUER-MAGNETE Vacodym, Vacomax data sheet," 2016.
- [9] C. Mi, G. Slemon, and R. Bonert, "Minimization of iron losses of permanent magnet synchronous machines," *Energy Conversion, IEEE Transactions on*, vol. 20, pp. 121–127, March 2005.
- [10] J. Pyrhonen, T. Jokinen, and V. Hrabovcova, *Design of Rotating Electrical Machines*. John Wiley & Sons, 2009.
- [11] V.-G. V. und Chemieingenieurwesen, *VDI Heat Atlas*. Springer reference, Springer, 2010.
- [12] M. Jaritz and J. Biela, "Analytical model for the thermal resistance of windings consisting of solid or litz wire," in *Power Electronics and Applications (EPE), 2013 15th European Conference on*, pp. 1–10, Sept 2013.